

Measurement of the Decays $B \rightarrow \eta \ell \nu_\ell$ and $B \rightarrow \eta' \ell \nu_\ell$ in Fully Reconstructed Events at Belle

C. Beleño,³¹ J. Dingfelder,⁷⁷ P. Urquijo,²³ H. Aihara,⁶⁹ S. Al Said,^{63,11} D. M. Asner,⁵⁴ T. Aushev,⁴³ R. Ayad,⁶³ V. Babu,⁶⁴ I. Badhrees,^{63,10} A. M. Bakich,⁶² V. Bansal,⁵⁴ P. Behera,¹ B. Bhuyan,⁴⁰ J. Biswal,⁶ A. Bobrov,^{25,52} M. Bračko,^{21,6} T. E. Browder,³⁵ D. Červenkov,²⁶ A. Chen,⁴⁷ B. G. Cheon,³⁴ R. Chistov,^{16,42} K. Cho,¹² S.-K. Choi,³³ Y. Choi,⁶¹ D. Cinabro,⁷⁴ N. Dash,³⁹ S. Di Carlo,⁷⁴ Z. Doležal,²⁶ S. Eidelman,^{25,52} H. Farhat,⁷⁴ J. E. Fast,⁵⁴ T. Ferber,²⁹ A. Frey,³¹ B. G. Fulsom,⁵⁴ V. Gaur,⁶⁴ N. Gabyshev,^{25,52} A. Garmash,^{25,52} R. Gillard,⁷⁴ P. Goldenzweig,⁸ T. Hara,^{36,32} H. Hayashii,⁴⁶ M. T. Hedges,³⁵ W.-S. Hou,⁴⁹ T. Iijima,^{45,44} K. Inami,⁴⁴ G. Inguglia,²⁹ A. Ishikawa,⁶⁷ R. Itoh,^{36,32} Y. Iwasaki,³⁶ H. B. Jeon,¹⁴ Y. Jin,⁶⁹ D. Joffe,⁹ K. K. Joo,²⁷ K. H. Kang,¹⁴ G. Karyan,²⁹ D. Y. Kim,⁵⁹ J. B. Kim,¹³ K. T. Kim,¹³ M. J. Kim,¹⁴ Y. J. Kim,¹² K. Kinoshita,²⁸ P. Kodyš,²⁶ S. Korpar,^{21,6} D. Kotchetkov,³⁵ P. Križan,^{17,6} P. Krokovny,^{25,52} R. Kulasiri,⁹ I. S. Lee,³⁴ Y. Li,⁷³ L. Li Gioi,²² J. Libby,¹ D. Liventsev,^{73,36} M. Lubej,⁶ T. Luo,⁵⁵ M. Masuda,⁶⁸ T. Matsuda,⁴¹ D. Matvienko,^{25,52} K. Miyabayashi,⁴⁶ H. Miyata,⁵¹ H. K. Moon,¹³ T. Mori,⁴⁴ E. Nakano,⁵³ M. Nakao,^{36,32} T. Nanut,⁶ K. J. Nath,⁴⁰ M. Nayak,^{74,36} S. Nishida,^{36,32} S. Ogawa,⁶⁶ S. Okuno,⁷ H. Ono,^{50,51} B. Pal,²⁸ C.-S. Park,⁷⁶ C. W. Park,⁶¹ H. Park,¹⁴ T. K. Pedlar,¹⁹ R. Pestotnik,⁶ L. E. Piilonen,⁷³ M. Ritter,¹⁸ Y. Sakai,^{36,32} M. Salehi,^{20,18} S. Sandilya,²⁸ T. Sanuki,⁶⁷ O. Schneider,¹⁵ G. Schnell,^{24,38} C. Schwanda,³ Y. Seino,⁵¹ K. Senyo,⁷⁵ O. Seon,⁴⁴ M. E. Sevior,²³ V. Shebalin,^{25,52} T.-A. Shibata,⁷⁰ J.-G. Shiu,⁴⁹ F. Simon,^{22,65} E. Solovieva,^{16,43} M. Starič,⁶ T. Sumiyoshi,⁷¹ M. Takizawa,^{58,37,56} U. Tamponi,^{4,72} K. Tanida,⁵ F. Tenchini,²³ M. Uchida,⁷⁰ T. Uglov,^{16,43} Y. Unno,³⁴ S. Uno,^{36,32} Y. Usov,^{25,52} C. Van Hulse,²⁴ G. Varner,³⁵ K. E. Varvell,⁶² A. Vinokurova,^{25,52} V. Vorobyev,^{25,52} C. H. Wang,⁴⁸ M.-Z. Wang,⁴⁹ P. Wang,² Y. Watanabe,⁷ E. Widmann,⁶⁰ E. Won,¹³ Y. Yamashita,⁵⁰ H. Ye,²⁹ J. Yelton,³⁰ Y. Yook,⁷⁶ Z. P. Zhang,⁵⁷ V. Zhilich,^{25,52} V. Zhukova,⁴² V. Zhulanov,^{25,52} and A. Zupanc^{17,6}

(The Belle Collaboration)

¹Indian Institute of Technology Madras, Chennai 600036

²Institute of High Energy Physics, Chinese Academy of Sciences, Beijing 100049

³Institute of High Energy Physics, Vienna 1050

⁴INFN - Sezione di Torino, 10125 Torino

⁵Advanced Science Research Center, Japan Atomic Energy Agency, Naka 319-1195

⁶J. Stefan Institute, 1000 Ljubljana

⁷Kanagawa University, Yokohama 221-8686

⁸Institut für Experimentelle Kernphysik, Karlsruher Institut für Technologie, 76131 Karlsruhe

⁹Kennesaw State University, Kennesaw, Georgia 30144

¹⁰King Abdulaziz City for Science and Technology, Riyadh 11442

¹¹Department of Physics, Faculty of Science, King Abdulaziz University, Jeddah 21589

¹²Korea Institute of Science and Technology Information, Daejeon 305-806

¹³Korea University, Seoul 136-713

¹⁴Kyungpook National University, Daegu 702-701

¹⁵École Polytechnique Fédérale de Lausanne (EPFL), Lausanne 1015

¹⁶P.N. Lebedev Physical Institute of the Russian Academy of Sciences, Moscow 119991

¹⁷Faculty of Mathematics and Physics, University of Ljubljana, 1000 Ljubljana

¹⁸Ludwig-Maximilians University, 80539 Munich

¹⁹Luther College, Decorah, Iowa 52101

²⁰University of Malaya, 50603 Kuala Lumpur

²¹University of Maribor, 2000 Maribor

²²Max-Planck-Institut für Physik, 80805 München

²³School of Physics, University of Melbourne, Victoria 3010

²⁴University of the Basque Country UPV/EHU, 48080 Bilbao

²⁵Budker Institute of Nuclear Physics SB RAS, Novosibirsk 630090

²⁶Faculty of Mathematics and Physics, Charles University, 121 16 Prague

²⁷Chonnam National University, Kwangju 660-701

²⁸University of Cincinnati, Cincinnati, Ohio 45221

²⁹Deutsches Elektronen-Synchrotron, 22607 Hamburg

³⁰University of Florida, Gainesville, Florida 32611

³¹II. Physikalisches Institut, Georg-August-Universität Göttingen, 37073 Göttingen

- ³²*SOKENDAI (The Graduate University for Advanced Studies), Hayama 240-0193*
³³*Gyeongsang National University, Chinju 660-701*
³⁴*Hanyang University, Seoul 133-791*
³⁵*University of Hawaii, Honolulu, Hawaii 96822*
³⁶*High Energy Accelerator Research Organization (KEK), Tsukuba 305-0801*
³⁷*J-PARC Branch, KEK Theory Center, High Energy Accelerator Research Organization (KEK), Tsukuba 305-0801*
³⁸*IKERBASQUE, Basque Foundation for Science, 48013 Bilbao*
³⁹*Indian Institute of Technology Bhubaneswar, Satya Nagar 751007*
⁴⁰*Indian Institute of Technology Guwahati, Assam 781039*
⁴¹*University of Miyazaki, Miyazaki 889-2192*
⁴²*Moscow Physical Engineering Institute, Moscow 115409*
⁴³*Moscow Institute of Physics and Technology, Moscow Region 141700*
⁴⁴*Graduate School of Science, Nagoya University, Nagoya 464-8602*
⁴⁵*Kobayashi-Maskawa Institute, Nagoya University, Nagoya 464-8602*
⁴⁶*Nara Women's University, Nara 630-8506*
⁴⁷*National Central University, Chung-li 32054*
⁴⁸*National United University, Miao Li 36003*
⁴⁹*Department of Physics, National Taiwan University, Taipei 10617*
⁵⁰*Nippon Dental University, Niigata 951-8580*
⁵¹*Niigata University, Niigata 950-2181*
⁵²*Novosibirsk State University, Novosibirsk 630090*
⁵³*Osaka City University, Osaka 558-8585*
⁵⁴*Pacific Northwest National Laboratory, Richland, Washington 99352*
⁵⁵*University of Pittsburgh, Pittsburgh, Pennsylvania 15260*
⁵⁶*Theoretical Research Division, Nishina Center, RIKEN, Saitama 351-0198*
⁵⁷*University of Science and Technology of China, Hefei 230026*
⁵⁸*Showa Pharmaceutical University, Tokyo 194-8543*
⁵⁹*Soongsil University, Seoul 156-743*
⁶⁰*Stefan Meyer Institute for Subatomic Physics, Vienna 1090*
⁶¹*Sungkyunkwan University, Suwon 440-746*
⁶²*School of Physics, University of Sydney, New South Wales 2006*
⁶³*Department of Physics, Faculty of Science, University of Tabuk, Tabuk 71451*
⁶⁴*Tata Institute of Fundamental Research, Mumbai 400005*
⁶⁵*Excellence Cluster Universe, Technische Universität München, 85748 Garching*
⁶⁶*Toho University, Funabashi 274-8510*
⁶⁷*Department of Physics, Tohoku University, Sendai 980-8578*
⁶⁸*Earthquake Research Institute, University of Tokyo, Tokyo 113-0032*
⁶⁹*Department of Physics, University of Tokyo, Tokyo 113-0033*
⁷⁰*Tokyo Institute of Technology, Tokyo 152-8550*
⁷¹*Tokyo Metropolitan University, Tokyo 192-0397*
⁷²*University of Torino, 10124 Torino*
⁷³*Virginia Polytechnic Institute and State University, Blacksburg, Virginia 24061*
⁷⁴*Wayne State University, Detroit, Michigan 48202*
⁷⁵*Yamagata University, Yamagata 990-8560*
⁷⁶*Yonsei University, Seoul 120-749*
⁷⁷*University of Bonn, 53115 Bonn*

We report branching fraction measurements of the decays $B^+ \rightarrow \eta\ell^+\nu_\ell$ and $B^+ \rightarrow \eta'\ell^+\nu_\ell$ based on 711 fb^{-1} of data collected near the $\Upsilon(4S)$ resonance with the Belle experiment at the KEKB asymmetric-energy e^+e^- collider. This data sample contains 772 million $B\bar{B}$ events. One of the two B mesons is fully reconstructed in a hadronic decay mode. Among the remaining (“signal- B ”) daughters, we search for the η meson in two decay channels, $\eta \rightarrow \gamma\gamma$ and $\eta \rightarrow \pi^+\pi^-\pi^0$, and reconstruct the η' meson in $\eta' \rightarrow \eta\pi^+\pi^-$ with subsequent decay of the η into $\gamma\gamma$. Combining the two η modes and using an extended maximum likelihood, the $B^+ \rightarrow \eta\ell^+\nu_\ell$ branching fraction is measured to be $(4.2 \pm 1.1(\text{stat.}) \pm 0.3(\text{syst.})) \times 10^{-5}$. For $B^+ \rightarrow \eta'\ell^+\nu_\ell$, we observe no significant signal and set an upper limit of 0.72×10^{-4} at 90% confidence level.

PACS numbers: 13.20.He, 14.40.Nd

The magnitude of the Cabibbo-Kobayashi-Maskawa matrix element $|V_{ub}|$ [1, 2] can be determined by *inclusive* measurements sensitive to the entire $b \rightarrow ul\nu_\ell$ rate in a given region of phase space, or by *exclusive* mea-

surements of specific $b \rightarrow u$ decays such as $B \rightarrow \pi l\nu_\ell$. As both experimental and theoretical uncertainties differ in the two approaches, consistency between the inclusive and exclusive determinations of $|V_{ub}|$ is a crucial cross-

check of our understanding of the CKM mechanism. At present, inclusive and exclusive measurements of $|V_{ub}|$ disagree by about three standard deviations [3]. Precise measurements of $B \rightarrow \eta \ell \nu_\ell$ and $B \rightarrow \eta' \ell \nu_\ell$ rates will improve the inclusive signal modelling, since the lack of knowledge on all exclusive $b \rightarrow u \ell \nu$ decays is one of the contributions to the systematic uncertainty [4]. Also, a measurement of the ratio $\mathcal{B}(B \rightarrow \eta \ell \nu_\ell)/\mathcal{B}(B \rightarrow \eta' \ell \nu_\ell)$ determines the $\eta - \eta'$ mixing angle and the $F_+^{B \rightarrow \eta(\eta')}$ form factor [5, 6] by constraining the gluonic singlet contribution to this form factor in the LCSR calculation [4]. In this paper, we report measurements of the branching fractions $\mathcal{B}(B^+ \rightarrow \eta \ell^+ \nu_\ell)$ and $\mathcal{B}(B^+ \rightarrow \eta' \ell^+ \nu_\ell)$ [7], where ℓ stands for either an electron or a muon. These are the first measurements of these decays based on the Belle data sample. The modes have been studied previously by CLEO [8, 9] and BaBar [10–13].

The Belle detector is a large-solid-angle magnetic spectrometer that consists of a silicon vertex detector (SVD), a 50-layer central drift chamber (CDC), an array of aerogel threshold Cherenkov counters (ACC), a barrel-like arrangement of time-of-flight scintillation counters (TOF), and an electromagnetic calorimeter comprised of CsI(Tl) crystals (ECL) located inside a super-conducting solenoid coil that provides a 1.5 T magnetic field. An iron flux-return located outside of the coil is instrumented to detect K_L^0 mesons and to identify muons (KLM). The detector is described in detail elsewhere [14].

In this analysis, we use the entire Belle data sample of 711 fb^{-1} collected at the KEKB asymmetric-energy e^+e^- collider [15] at the center-of-mass (c.m.) energy of the $\Upsilon(4S)$ resonance. The sample contains $(772 \pm 11) \times 10^6 e^+e^- \rightarrow \Upsilon(4S) \rightarrow B\bar{B}$ events. Two inner detector configurations were used in the course of the experiment. A 2.0 cm beampipe and a 3-layer silicon vertex detector were used for the first sample of $152 \times 10^6 B\bar{B}$ pairs, while a 1.5 cm beampipe, a 4-layer silicon detector, and a small-cell inner drift chamber were used to record the remaining $620 \times 10^6 B\bar{B}$ pairs [16].

Monte Carlo (MC) simulated samples are generated using the EvtGen [17] package and the response of the detector is modeled using GEANT3 [18]. MC samples equivalent to about five times the integrated luminosity are produced for $\Upsilon(4S) \rightarrow B\bar{B}$ events and $e^+e^- \rightarrow q\bar{q}$ continuum events, where q stands for a u , d , s or c quark. Simulated samples containing the decay $b \rightarrow u \ell \nu$ equivalent to 20 times the integrated luminosity are used in this analysis. In these samples, the decays $B^+ \rightarrow \eta \ell^+ \nu_\ell$ and $B^+ \rightarrow \eta' \ell^+ \nu_\ell$ have been generated according to the ISWG2 [19] calculation of the form factors.

After selecting hadronic events ($\Upsilon(4S) \rightarrow B\bar{B}$, $e^+e^- \rightarrow q\bar{q}$) based on the charged track multiplicity and the total visible energy [20], we reconstruct one B meson (B_{tag}) of the $B\bar{B}$ pair in a hadronic decay mode using the Belle full reconstruction software [21] based on the

NeuroBayes neural-network package [22]. A total of 1104 exclusive decay channels to charm mesons and 71 neural networks were employed to reconstruct B_{tag} whose quality is characterized by the NeuroBayes classifier (O_{NB}), which ranges from 0 to 1. We require that $\ln O_{NB} > -8$ to ensure good quality of B_{tag} . B_{tag} is identified using the beam-constrained mass, $M_{\text{bc}} = \sqrt{E_{\text{beam}}^*{}^2 - |\vec{p}_{B_{\text{tag}}}^*|^2}$, and the energy difference, $\Delta E = E_{B_{\text{tag}}}^* - E_{\text{beam}}^*$, where E_{beam}^* is the energy of the colliding beam particles in the c.m. frame and $E_{B_{\text{tag}}}^*$ and $\vec{p}_{B_{\text{tag}}}^*$ are the reconstructed energy and three-momentum of the B_{tag} candidate in the same reference system [23]. For well-reconstructed candidates, ΔE peaks at zero and M_{bc} peaks at the nominal B mass; we retain events that satisfy $-0.1 \text{ GeV} < \Delta E < 0.05 \text{ GeV}$ and $5.27 \text{ GeV} < M_{\text{bc}} < 5.29 \text{ GeV}$. Finally, we select only the charged B_{tag} candidates since the signal mode only involves charged B mesons.

The other B meson in the event, B_{sig} , is reconstructed using all charged particles and neutral clusters not associated with the B_{tag} candidate. Low-momentum particles, which spiral inside the CDC and pass close to the interaction point, can lead to multiple reconstruction of the same particle. Duplicate tracks are identified as pairs of tracks with momenta transverse to the beam direction below 275 MeV, with a momentum difference below 100 MeV, and with an opening angle either below 15° or above 165° . Whenever such pair is found, we select the track passing closer to the interaction point.

Charged hadrons are identified using the ionization energy loss dE/dx in the CDC, the time-of-flight information provided by the TOF, and the response of the ACC [24]. Pions used in this analysis are identified with an efficiency of 98% and a kaon fake rate of 30%. Electron candidates are identified using the ratio of the energy detected in the ECL to the track momentum, the ECL shower shape, the position matching between the track and the ECL cluster, the energy loss in the CDC, and the response of the ACC. Muons are identified based on their penetration range and transverse scattering in the KLM detector. In the momentum region relevant to this analysis, charged leptons are identified with an efficiency of about 90% and the probability to misidentify a pion as an electron (muon) is 0.25% (1.4%) [25, 26]. We veto charged leptons from photon conversion and J/ψ decay if the lepton candidate, when combined with an oppositely charged particle, gives an invariant mass below 100 MeV or within ± 4.9 MeV around the nominal J/ψ mass. Only events with a single charged lepton candidate on the signal side are considered in this analysis.

Photons are reconstructed from clusters in the ECL not matched to a track. Beam-related background is removed by rejecting clusters with an energy below 50 MeV. Higher thresholds of 100 MeV and 150 MeV are applied in the forward ($17^\circ < \theta < 32^\circ$) and backward ($130^\circ < \theta < 150^\circ$) regions, respectively, where θ is the

laboratory-frame polar angle with respect to the opposite of the positron beam direction. Neutral pion candidates are reconstructed by combining two photons, requiring their invariant mass to lie between 120 and 150 MeV. The c.m. momentum of the π^0 candidate must exceed 200 MeV.

Then, η mesons are reconstructed in the decays $\eta \rightarrow \gamma\gamma$ and $\eta \rightarrow \pi^+\pi^-\pi^0$. Candidates are selected in the intervals $0.506 \text{ GeV} < M_{\gamma\gamma} < 0.584 \text{ GeV}$ and $0.535 \text{ GeV} < M_{\pi^+\pi^-\pi^0} < 0.560 \text{ GeV}$, determined by signal-to-background optimization on MC simulated events. We reconstruct η' candidates in the $\eta' \rightarrow \eta\pi^+\pi^-$ channel with $\eta \rightarrow \gamma\gamma$ and require $0.926 \text{ GeV} < M_{\eta\pi^+\pi^-} < 0.986 \text{ GeV}$. The aforementioned mass requirements correspond to 3σ windows around the nominal mass of the mesons. The fraction of events with multiple meson candidates after the signal selection corresponds to 17.5% for $\eta \rightarrow \gamma\gamma$, 7.4% for $\eta \rightarrow \pi^+\pi^-\pi^0$ and 36% for $\eta' \rightarrow \eta(\gamma\gamma)\pi^+\pi^-$. If more than one $\eta^{(\prime)}$ candidate is found on the signal side, we select the one closer to the nominal $\eta^{(\prime)}$ mass [27]. For modes involving charged pions, we also use information on the signal vertex quality, and choose the candidate with the smallest χ^2_{tot} defined as $\chi^2_{\text{mass}} + \chi^2_{\text{vertex}}$.

After selecting the single charged lepton and the $\eta^{(\prime)}$ candidate, the remaining particles on the signal side are considered further to reduce background. We require no remaining charged particles. The sum of the energies of neutral clusters associated with neither B_{tag} nor B_{sig} must be below 0.5 GeV. To reject charged leptons inconsistent with the signal decay, the charge of the lepton must be opposite to that of the B_{tag} meson. Since the $\eta \rightarrow \gamma\gamma$ mode has a larger background than the $\eta \rightarrow \pi^+\pi^-\pi^0$ mode, we remove any events in the former channel that contain one or more neutral pions on the signal side. This π^0 veto is not applied to the $\eta' \rightarrow \eta(\gamma\gamma)\pi^+\pi^-$ channel.

The $B \rightarrow \eta^{(\prime)}\ell\nu_\ell$ yield is extracted from the distribution of the missing mass squared, defined as $M_{\text{miss}}^2 = (p_{B_{\text{tag}}} - p_{\eta^{(\prime)}} - p_\ell)^2$, where $p_{B_{\text{tag}}}$, $p_{\eta^{(\prime)}}$ and p_ℓ are the four-momenta of the B_{tag} , $\eta^{(\prime)}$, and charged lepton candidates, respectively. For well-reconstructed signal decays, we expect M_{miss}^2 to peak at zero, as the only remaining particle in the event is the neutrino. We determine the yields of the signal, $b \rightarrow ul\nu_\ell$, $b \rightarrow cl\nu_\ell$ and continuum backgrounds from an extended binned maximum likelihood fit to the M_{miss}^2 distribution between -1.6 and 5.0 GeV^2 (with a bin width of 0.2 GeV^2). The shapes of the fit components are taken from MC simulation and the fitting algorithm accounts for statistical fluctuations in both the real data and the MC simulated samples [28]. As continuum is a small component, we fix it to the MC expected yield. The contributions from secondary and fake leptons are negligible and thus not taken into account as additional fit components. For $B^+ \rightarrow \eta\ell\nu_\ell$, the fit incorporates both η modes. As a cross-check, we

also determine the fit results for the individual η modes. In addition, we include also fit results for the regions of $q^2 = (p_\ell + p_{\nu_\ell})^2$ below and above 12 GeV^2 . These fit results are quoted in Table I and shown in Fig. 1. We carried out 10000 toy MC to validate the fit procedure. The distributions of signal and background in each ensemble are generated according to their measured values in data, and then the fit procedure is executed. The statistical uncertainties estimated by the nominal fit are consistent with the size of the uncertainties evaluated by the toy MC technique. However, given that in some channels the pull distribution exhibits a non-Gaussian shape, we do not apply a correction to the central value of the signal yields. Instead, we assign a systematic uncertainty associated with the fit procedure with values between 2% and 10% depending on the reconstructed channel.

The signal branching fractions are calculated as

$$\mathcal{B}(B^+ \rightarrow \eta^{(\prime)}\ell^+\nu_\ell) = \frac{1}{2} \frac{N_{\text{signal}}}{N_{B\bar{B}} \mathcal{B}(\eta^{(\prime)}) \epsilon}, \quad (1)$$

where N_{signal} is the fitted signal yield from Table I, $N_{B\bar{B}}$ is the number of $B\bar{B}$ pairs in the Belle data, $\mathcal{B}(\eta^{(\prime)})$ is the world average value of the $\eta^{(\prime)}$ sub-decay branching fraction [27, 29] and ϵ is the signal efficiency including B_{tag} reconstruction, calibrated as described in Ref. [30]. The factor of 2 in the denominator indicates an average over lepton flavor. The combined and separate $B^+ \rightarrow \eta\ell^+\nu_\ell$ branching fractions are quoted in Table II. Our result for the $B^+ \rightarrow \eta\ell^+\nu_\ell$ branching fraction is $(4.2 \pm 1.1(\text{stat}) \pm 0.3(\text{syst})) \times 10^{-5}$. The significance of the observed signal [31, 32] is calculated as $S = \sqrt{-2\Delta \ln(\mathcal{L})}$ with $\Delta \ln(\mathcal{L}) = \ln(\mathcal{L}_B) - \ln(\mathcal{L}_{S+B})$, where $\ln(\mathcal{L}_{S+B})$ is the maximized log-likelihood assuming a signal plus background hypothesis and $\ln(\mathcal{L}_B)$ is the maximized log-likelihood with background only. Systematic uncertainties are included by convolving \mathcal{L} with a Gaussian function of width corresponding to the systematic uncertainty in the number of signal events. The signal significance in the combined η mode sample is found to be $S = 3.7$, including systematic uncertainties related to the signal yield.

For $B^+ \rightarrow \eta'\ell^+\nu_\ell$, we calculate a branching fraction of $(3.6 \pm 2.7(\text{stat.})^{+0.3}_{-0.4}(\text{syst.})) \times 10^{-5}$ and a significance (including systematics) of $S = 1.6$. Given the low value of S , we convert this result into an upper limit on $\mathcal{B}(B^+ \rightarrow \eta'\ell^+\nu_\ell)$. Using the frequentist calculator from the RooStats package [33], we obtain a 90% confidence level upper limit of 11.6 events on the $B^+ \rightarrow \eta'\ell^+\nu_\ell$ signal yield or 0.72×10^{-4} on the branching fraction. For the $B^+ \rightarrow \eta\ell^+\nu_\ell$ channel this upper limit is of 51.2 events, corresponding an upper bound on the branching ratio of 0.55×10^{-4} .

We also determine the ratio $\mathcal{B}(B^+ \rightarrow \eta'\ell^+\nu_\ell)/\mathcal{B}(B^+ \rightarrow \eta\ell^+\nu_\ell)$ to be $0.86 \pm 0.68(\text{stat.}) \pm 0.09(\text{syst.})$, which is important to constraint the gluonic singlet contribution [4]. A 90% confidence level upper limit to the latter quantity

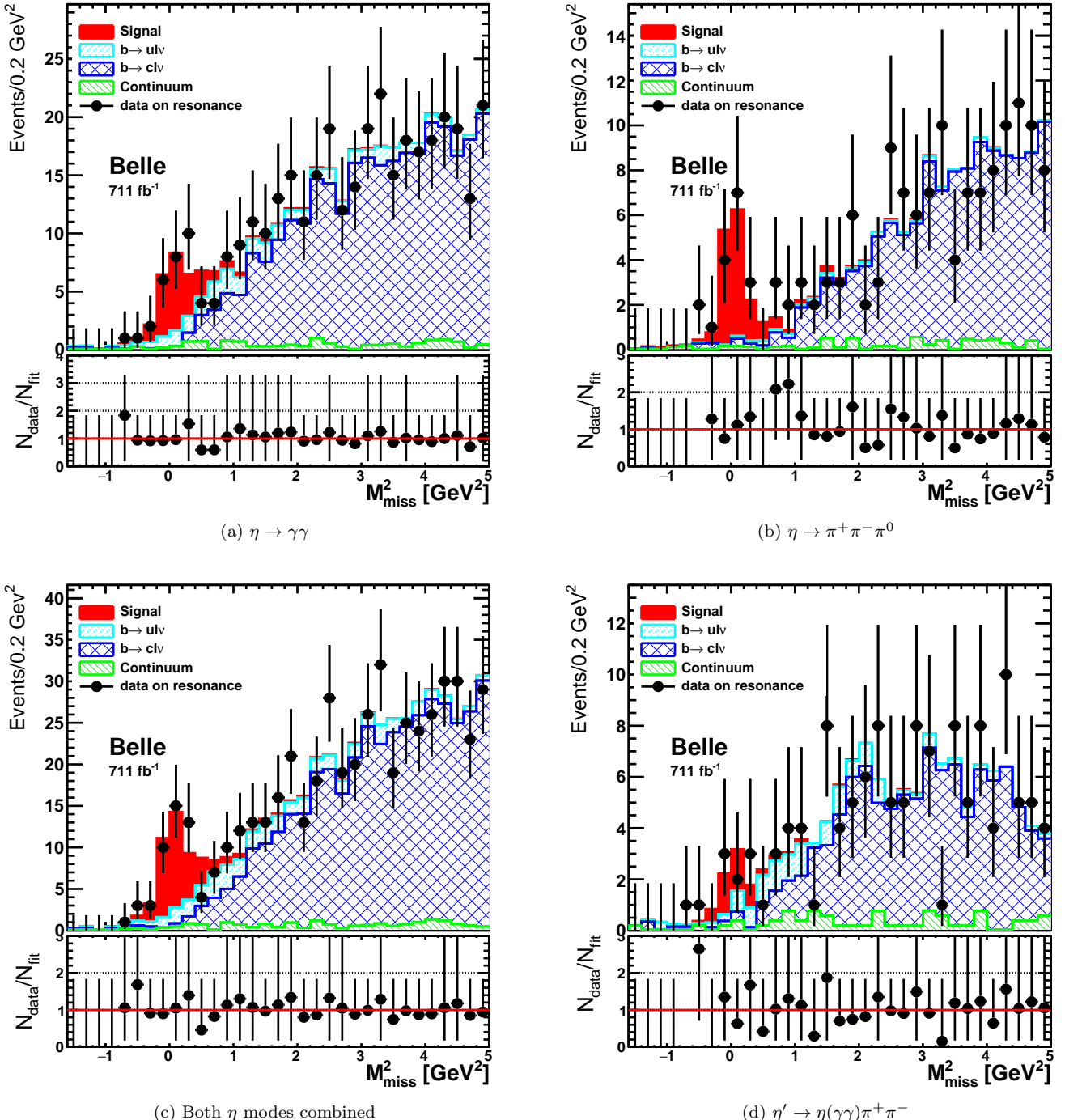


FIG. 1: Distribution of M_{miss}^2 (points with error bars) for: (a) $\eta \rightarrow \gamma\gamma$, (b) $\eta \rightarrow \pi^+\pi^-\pi^0$, (c) both η modes combined, and (d) $\eta' \rightarrow \eta(\gamma\gamma)\pi^+\pi^-$. The fit results with the different components are shown as the colored histograms. The ratio of data to the sum of the fitted yields is shown below each plot.

is calculated to be $\mathcal{B}(B^+ \rightarrow \eta'\ell^+\nu_\ell)/\mathcal{B}(B^+ \rightarrow \eta\ell^+\nu_\ell) < 1.31$.

We compute the CKM matrix element $|V_{ub}|$ from our measurement of $\mathcal{B}(B^+ \rightarrow \eta\ell^+\nu_\ell)$ in the region $q^2 < 12 \text{ GeV}^2$ using the light-cone sum rule (LCSR) calculation

of the form factor $f_+(q^2)$ in Ref. [4]. For that purpose we use the relation:

TABLE I: Fit results in regions of $q^2 = (p_\ell + p_{\nu_\ell})^2$ for the different modes. “Raw yield” denotes the number of events seen in the data; “signal”, “ $b \rightarrow u\ell\nu_\ell$ ”, “ $b \rightarrow c\ell\nu_\ell$ ” and “continuum” are the fitted yields. The continuum component is fixed and hence no fit errors are quoted. Only statistical uncertainties are shown.

| Channel | $B^+ \rightarrow \eta\ell\nu_\ell$ | | | | | | | | | $B^+ \rightarrow \eta'\ell\nu_\ell$ |
|-------------------------------|------------------------------------|----------------|---------------|------------------------------------|----------------|---------------|---------------------|----------------|----------------|-------------------------------------|
| | $\eta \rightarrow \gamma\gamma$ | | | $\eta \rightarrow \pi^+\pi^-\pi^0$ | | | Both modes combined | | | |
| Mode | All | < 12 | > 12 | All | < 12 | > 12 | All | < 12 | > 12 | All |
| q^2 [GeV 2] | All | < 12 | > 12 | All | < 12 | > 12 | All | < 12 | > 12 | All |
| Raw yield | 355 | 261 | 94 | 148 | 98 | 50 | 503 | 359 | 144 | 129 |
| Signal | 23.6 ± 8.7 | 15.7 ± 7.3 | 9.0 ± 5.3 | 16.0 ± 5.3 | 12.2 ± 4.1 | 4.0 ± 2.5 | 38.8 ± 10.1 | 27.9 ± 8.7 | 12.9 ± 6.1 | 5.7 ± 4.4 |
| $b \rightarrow u\ell\nu_\ell$ | 32 ± 25 | 22 ± 27 | 10 ± 13 | 4 ± 21 | 1 ± 5 | 4 ± 8 | 46 ± 29 | 30 ± 29 | 14 ± 18 | 15 ± 13 |
| $b \rightarrow c\ell\nu_\ell$ | 287 ± 27 | 212 ± 28 | 73 ± 13 | 122 ± 17 | 79 ± 10 | 41 ± 10 | 399 ± 31 | 285 ± 30 | 114 ± 18 | 99 ± 14 |
| Continuum | 12.7 | 10.4 | 2.3 | 6.2 | 5.2 | 0.9 | 18 | 15.7 | 3.2 | 9.7 |
| ϵ [10 $^{-3}$] | 1.21 | 1.28 | 0.99 | 0.53 | 0.57 | 0.44 | 0.96 | 1.02 | 0.79 | 0.61 |
| χ^2/ndf | 12.0/29 | 11.5/29 | 35.2/29 | 18.8/29 | 30.5/29 | 19.4/29 | 18.0/29 | 20.1/29 | 35.5/29 | 24.4/29 |
| Probability[%] | 99.8 | 99.8 | 19.0 | 92.5 | 39.1 | 91.1 | 94.4 | 88.8 | 18.9 | 70.9 |

TABLE II: Branching fraction of the decay $B^+ \rightarrow \eta\ell^+\nu_\ell$ (in units of 10 $^{-5}$) calculated for the different samples and regions of q^2 . The first error is statistical and the second is systematic. The main result is the lower right value (Combined, All q^2). The values in the “Sum” row provide a cross-check.

| | $\eta \rightarrow \gamma\gamma$ | $\eta \rightarrow \pi^+\pi^-\pi^0$ | Combined |
|---------------------|---------------------------------|------------------------------------|---|
| $q^2 < 12$ GeV 2 | $2.0 \pm 0.9 \pm 0.2$ | $6.0 \pm 2.0 \pm 0.6$ | $2.8 \pm 0.9 \pm 0.2$ |
| $q^2 > 12$ GeV 2 | $1.5 \pm 0.9 \pm 0.1$ | $2.6 \pm 1.6 \pm 0.3$ | $1.7 \pm 0.8 \pm 0.1$ |
| Sum | $3.5 \pm 1.3 \pm 0.3$ | $8.6 \pm 2.6 \pm 0.7$ | $4.5 \pm 1.2 \pm 0.3$ |
| All q^2 | $3.4 \pm 1.2 \pm 0.3$ | $8.5 \pm 2.8^{+0.7}_{-0.8}$ | $4.2 \pm 1.1 \pm 0.3$ |

$$|V_{ub}| = \sqrt{\frac{C_v \Delta \mathcal{B}}{\tau_B \Delta \zeta}}, \quad (2)$$

where $C_v = 2$ for B^+ decays, $\Delta \mathcal{B}$ is the measured partial branching ratio for $q^2 < 12$ GeV 2 , $\tau_B = 1.638(4)$ ps [27] is the lifetime of the B^+ meson and $\Delta \zeta$ is the decay rate provided by theory [4]. We determine $\Delta \zeta$ to be $(2.65^{+0.43}_{-0.47}) \times 10^{12}$ s $^{-1}$ and consequently $|V_{ub}| = (3.59 \pm 0.58\text{stat.}) \pm 0.13\text{(syst.)}^{+0.29}_{-0.32}\text{(theo.)} \times 10^{-3}$, which is in agreement with previous exclusive measurements [3].

The systematic uncertainties considered for the branching fractions are summarized in Table III and fall into two groups: those related to detector performance and those in the signal and background modeling. Uncertainties related to detector performance are derived from dedicated studies of control samples within the Belle experiment to measure the tracking efficiency of charged particles, the photon and neutral-pion reconstruction efficiency, and the charged-lepton and pion-identification efficiency. Systematic uncertainties related to the signal and background model are estimated by varying the

respective parameter in the simulation within its uncertainty or by reweighting MC samples. The deviation of the result from the nominal fit is taken as the uncertainty.

Uncertainties in the signal form factors are estimated by comparing the Ball-Zwicky model [34] to the ISGW2 model [19]. The form factor parameters of the former are taken from Ref. [4]. The HQET-based form factors of the decays $B \rightarrow D^{(*)}\ell\nu_\ell$ in the MC simulation are adjusted to the recent world average values [3]. The branching fractions of $B \rightarrow (D^{(*)}, \pi, \rho, \omega)\ell\nu_\ell$ have been corrected [27]. The hadronic branching fractions on the tag side are adjusted by the B_{tag} calibration and its uncertainty is taken from Ref. [30]. We vary the branching fractions of the $b \rightarrow u\ell\nu_\ell$ and $b \rightarrow c\ell\nu_\ell$ decay modes within ± 1 standard deviation of their world average values. We consider the form-factor uncertainties in the decays $B \rightarrow D^*\ell\nu_\ell$, $B \rightarrow D^0\ell\nu_\ell$, $B \rightarrow \pi\ell\nu_\ell$, and $B \rightarrow \omega\ell\nu_\ell$, and uncertainties in the shape-function parameters of the inclusive $b \rightarrow u\ell\nu_\ell$ model. We further assign an uncertainty due to the branching fraction uncertainty in the $\eta^{(\prime)}$ sub-decay modes. The systematic error components in which a weight factor is applied include uncertainties due to secondary and fake leptons and the continuum.

The contribution of the secondary leptons is adjusted to the measured $b \rightarrow c \rightarrow \ell$ branching fraction. The contribution of events in which a lepton has been misidentified as a hadron is corrected using the fake rate measured in a kinematically selected $D^{*+} \rightarrow D^0(K^-\pi^+)\pi^+$ sample. Since the expected number of continuum events is small after signal selection, a comparison with off-resonance data is not carried out. Instead, we rely on MC simulation to estimate the systematic uncertainty associated with continuum normalization by varying the number of events by 20% and examining the effect on the fit. The deviation from the nominal fit is taken as the uncertainty. The uncertainty on the number of produced B -meson pairs is 1.4%.

In summary, we have measured the branching fraction of the decay $B^+ \rightarrow \eta\ell^+\nu_\ell$ to be $(4.2 \pm 1.1 \pm 0.3) \times 10^{-5}$, where the first error is statistical and the second systematic. For the branching fraction of $B^+ \rightarrow \eta'\ell^+\nu_\ell$, we determine a 90% confidence level upper limit of 0.72×10^{-4} . The measurements are compatible with previous analyses performed by CLEO and BaBar [8–13]. Our measurement is limited by the size of the Belle data sample. Significant improvements can thus be expected from the Belle II/SuperKEKB super flavor factory.

We thank the KEKB group for the excellent operation of the accelerator; the KEK cryogenics group for the efficient operation of the solenoid; and the KEK computer group, the National Institute of Informatics, and the PNNL/EMSL computing group for valuable computing and SINET5 network support. We acknowledge support from the Ministry of Education, Culture, Sports, Science, and Technology (MEXT) of Japan, the Japan Society for the Promotion of Science (JSPS), and the Tau-Lepton Physics Research Center of Nagoya University; the Australian Research Council; Austrian Science Fund under Grant No. P 26794-N20; the National Natural Science Foundation of China under Contracts No. 10575109, No. 10775142, No. 10875115, No. 11175187, No. 11475187, No. 11521505 and No. 11575017; the Chinese Academy of Science Center for Excellence in Particle Physics; the Ministry of Education, Youth and Sports of the Czech Republic under Contract No. LG14034; the Carl Zeiss Foundation, the Deutsche Forschungsgemeinschaft, the Excellence Cluster Universe, and the VolkswagenStiftung; the Department of Science and Technology of India; the Istituto Nazionale di Fisica Nucleare of Italy; the WCU program of the Ministry of Education, National Research Foundation (NRF) of Korea Grants No. 2011-0029457, No. 2012-0008143, No. 2014R1A2A2A01005286, No. 2014R1A2A2A01002734, No. 2015R1A2A2A01003280, No. 2015H1A2A1033649, No. 2016R1D1A1B01010135, No. 2016K1A3A7A09005603, No. 2016K1A3A7A09005604, No. 2016R1D1A1B02012900,

No. 2016K1A3A7A09005606, No. NRF-2013K1A3A7A06056592; the Brain Korea 21-Plus program and Radiation Science Research Institute; the Polish Ministry of Science and Higher Education and the National Science Center; the Ministry of Education and Science of the Russian Federation and the Russian Foundation for Basic Research; the Slovenian Research Agency; Ikerbasque, Basque Foundation for Science and the Euskal Herriko Unibertsitatea (UPV/EHU) under program UFI 11/55 (Spain); the Swiss National Science Foundation; the Ministry of Education and the Ministry of Science and Technology of Taiwan; and the U.S. Department of Energy and the National Science Foundation.

-
- [1] M. Kobayashi and T. Maskawa, Prog. Theor. Phys. **49**, 652 (1973).
- [2] N. Cabibbo, Phys. Rev. Lett. **10**, 531 (1963).
- [3] Y. Amhis *et al.* (Heavy Flavor Averaging Group), arXiv:1612.07233 [hep-ex] and online updates at <http://www.slac.stanford.edu/xorg/hfag>.
- [4] P. Ball and G.W. Jones, J. High Energy Phys. **08**, 25 (2007).
- [5] C.S. Kim and Y.D. Yang, Phys. Rev. D **65**, 017501 (2001).
- [6] C.S. Kim, S. Oh and C. Yu, Phys. Lett. B **590**, 223 (2004).
- [7] Throughout this paper, the inclusion of the charge conjugate mode decay is implied unless stated otherwise.
- [8] R. Gray *et al.* (CLEO Collaboration), Phys. Rev. D **76**, 012007 (2007).
- [9] N. E. Adam *et al.* (CLEO Collaboration), Phys. Rev. Lett. **99**, 041802 (2007).
- [10] B. Aubert *et al.* (BaBar Collaboration), Phys. Rev. Lett. **101**, 081801 (2008).
- [11] B. Aubert *et al.* (BaBar Collaboration), Phys. Rev. D. **79**, 052011 (2009).
- [12] P. del Amo Sánchez *et al.* (BaBar Collaboration), Phys. Rev. D **83**, 052011 (2011).
- [13] J. P. Lees *et al.* (BaBar Collaboration), Phys. Rev. D **86**, 092004 (2012).
- [14] A. Abashian *et al.* (Belle Collaboration), Nucl. Instr. and Meth. A **479**, 117 (2002). See also detector section in J. Brodzicka *et al.*, Prog. Theor. Exp. Phys., 04D001 (2012).
- [15] S. Kurokawa and E. Kikutani, Nucl. Instr. and Meth. A **499**, 1 (2003), and other papers included in this volume. See also T. Abe *et al.*, Prog. Theor. Exp. Phys., 03A001 (2013).
- [16] Z. Natkaniec *et al.* (Belle SVD2 Group), Nucl. Instr. and Methods Phys. Res. A **560**, 1 (2006).
- [17] D. Lange, Nucl. Instr. Methods Phys. Res. A **462**, 152 (2001).
- [18] R. Brun *et al.*, CERN-DD-EE-84-1 (1985).
- [19] D. Scora and N. Isgur, Phys. Rev. D **52**, 2783 (1995).
- [20] K. Abe *et al.* (Belle Collaboration), Phys. Rev. D **64**, 072001 (2001).
- [21] M. Feindt *et al.*, Nucl. Instr. Methods Phys. Res. A **654**, 432 (2011).

TABLE III: Relative systematic uncertainties in the signal yield in per cent for the fits to the two η -mode samples and in the different q^2 regions.

| Mode q^2 [GeV 2] | $\eta \rightarrow \gamma\gamma$ | | | $\eta \rightarrow \pi^+\pi^-\pi^0$ | | | Both η modes | | | $\eta' \rightarrow \eta(\gamma\gamma)\pi^+\pi^-$ | |
|---|---------------------------------|--------------------|--------------------|------------------------------------|--------------------|--------------------|--------------------|-------------------|--------------------|--|--|
| | All | < 12 | > 12 | All | < 12 | > 12 | All | < 12 | > 12 | All | |
| Track finding | ± 0.35 | ± 0.35 | ± 0.35 | ± 1.05 | ± 1.05 | ± 1.05 | ± 0.5 | ± 0.5 | ± 0.5 | ± 1.05 | |
| Photon finding | ± 4.0 | ± 4.0 | ± 4.0 | ± 0.0 | ± 0.0 | ± 0.0 | ± 3.1 | ± 3.1 | ± 3.1 | ± 4.0 | |
| π^0 reconstruction | ± 0.0 | ± 0.0 | ± 0.0 | ± 2.5 | ± 2.5 | ± 2.5 | ± 0.5 | ± 0.5 | ± 0.5 | ± 0.0 | |
| π^0 veto | ± 2.5 | ± 2.5 | ± 2.5 | ± 0.0 | ± 0.0 | ± 0.0 | ± 2.0 | ± 2.0 | ± 2.0 | ± 0.0 | |
| Pion ID | ± 0.0 | ± 0.0 | ± 0.0 | ± 1.0 | ± 1.0 | ± 1.0 | ± 0.20 | ± 0.20 | ± 0.20 | ± 1.0 | |
| Lepton ID | ± 2.0 | ± 2.0 | ± 2.0 | ± 2.0 | ± 2.0 | ± 2.0 | ± 2.0 | ± 2.0 | ± 2.0 | ± 2.0 | |
| Lepton fake rate | ± 0.36 | $^{+0.19}_{-0.13}$ | ± 0.11 | $^{+0.46}_{-0.50}$ | $^{+0.42}_{-0.47}$ | $^{+0.18}_{-0.16}$ | $^{+0.47}_{-0.44}$ | ± 0.51 | $^{+0.02}_{-0.07}$ | $^{+1.6}_{-1.8}$ | |
| Signal model | ± 0.83 | ± 0.75 | ± 1.0 | ± 0.50 | ± 0.70 | ± 0.46 | ± 0.88 | ± 0.71 | ± 2.0 | ± 0.28 | |
| $b \rightarrow u\ell\nu_\ell$ form factors | ± 1.1 | ± 0.49 | ± 0.72 | $^{+1.8}_{-2.6}$ | $^{+0.14}_{-0.16}$ | $^{+0.82}_{-1.4}$ | $^{+0.31}_{-0.43}$ | $^{+0.73}_{-1.1}$ | $^{+0.77}_{-0.70}$ | $^{+0.92}_{-0.56}$ | |
| $b \rightarrow u\ell\nu_\ell$ branching fractions | $^{+0.26}_{-0.20}$ | ± 1.0 | $^{+1.4}_{-1.3}$ | $^{+0.04}_{-0.05}$ | ± 0.05 | $^{+0.85}_{-0.95}$ | $^{+0.50}_{-0.45}$ | $^{+1.5}_{-1.8}$ | $^{+0.86}_{-1.2}$ | $^{+1.9}_{-2.4}$ | |
| $b \rightarrow c\ell\nu_\ell$ form factors | $^{+1.0}_{-0.15}$ | $^{+2.3}_{-0.60}$ | ± 0.0 | $^{+0.21}_{-0.06}$ | $^{+0.70}_{-0.22}$ | ± 0.0 | $^{+1.1}_{-0.10}$ | $^{+1.3}_{-0.24}$ | ± 0.0 | $^{+0.18}_{-0.23}$ | |
| $b \rightarrow c\ell\nu_\ell$ branching fractions | ± 0.14 | ± 0.80 | ± 0.29 | ± 0.28 | $^{+0.43}_{-0.45}$ | $^{+0.18}_{-0.28}$ | ± 0.13 | ± 0.64 | $^{+0.21}_{-0.27}$ | ± 0.62 | |
| Secondary leptons | $^{+0.00}_{-0.06}$ | ± 0.12 | $^{+0.01}_{-0.03}$ | $^{+0.07}_{-0.04}$ | $^{+0.15}_{-0.13}$ | $^{+0.02}_{-0.12}$ | $^{+0.03}_{-0.01}$ | ± 0.08 | $^{+0.06}_{-0.04}$ | $^{+0.01}_{-0.00}$ | |
| $\mathcal{B}(\eta^{(\prime)})$ [29] | ± 0.50 | ± 0.50 | ± 0.50 | ± 1.2 | ± 1.2 | ± 1.2 | ± 0.50 | ± 0.50 | ± 0.50 | ± 1.7 | |
| Hadronic tag | ± 4.2 | ± 4.2 | ± 4.2 | ± 4.2 | ± 4.2 | ± 4.2 | ± 4.2 | ± 4.2 | ± 4.2 | ± 4.2 | |
| $N(B\bar{B})$ | ± 1.4 | ± 1.4 | ± 1.4 | ± 1.4 | ± 1.4 | ± 1.4 | ± 1.4 | ± 1.4 | ± 1.4 | ± 1.4 | |
| Continuum | $^{+0.77}_{-0.80}$ | $^{+0.98}_{-0.96}$ | $^{+0.24}_{-0.30}$ | $^{+0.66}_{-0.64}$ | $^{+1.1}_{-1.2}$ | $^{+0.71}_{-0.62}$ | ± 0.47 | ± 0.83 | $^{+1.2}_{-1.3}$ | ± 3.9 | |
| Fit procedure | ± 2.9 | ± 9.8 | ± 2.0 | ± 6.3 | ± 8.7 | ± 9.6 | ± 2.2 | ± 5.6 | ± 3.2 | ± 5.2 | |
| Total | ± 7.6 | $^{+12.3}_{-12.1}$ | ± 7.3 | $^{+8.8}_{-9.0}$ | ± 10.6 | $^{+11.3}_{-11.4}$ | ± 6.7 | ± 8.7 | $^{+7.4}_{-7.5}$ | $^{+9.7}_{-9.8}$ | |

- [22] M. Feindt and U. Kerzel, Nucl. Instr. Meth. A **559**, 190 (2006).
- [23] The use of natural units ($c = 1$) is assumed throughout the paper.
- [24] E. Nakano, Nucl. Instr. Methods Phys. Res. A **494**, 402 (2002).
- [25] K. Hanagaki *et al.*, Nucl. Instr. Methods Phys. Res. A **485**, 490 (2002).
- [26] A. Abashian *et al.*, Nucl. Instr. Methods Phys. Res. A **491**, 69 (2002).
- [27] C. Patrignani *et al.* (Particle Data Group), Chin. Phys. C **40**, 100001 (2016).
- [28] R. Barlow and C. Beeston, Comput. Phys. Commun. **77** 219 (1993).
- [29] For the combined sample, $\mathcal{B}(\eta)$ is the sum of the $\eta \rightarrow \gamma\gamma$ and $\eta \rightarrow \pi^+\pi^-\pi^0$ branching fractions.
- [30] A. Sibidanov *et al.* (Belle Collaboration), Phys. Rev. D **88**, 032005 (2013).
- [31] G.J. Feldman and R.D. Cousins, Phys. Rev. D **57**, 3873 (1998).
- [32] Yong-Sheng Zhu, High Energy Phys. Nucl. Phys. **30**, 331 (2006).
- [33] L. Moneta *et al.*, PoS (ACAT2010) **057**, (2010).
- [34] P. Ball and R. Zwicky, Phys. Rev. D **71**, 014015 (2005); P. Ball and R. Zwicky, Phys. Rev. D **71**, 014029 (2005).